AIP | Applied Physics Letters

Determination of thickness and composition of high-k dielectrics using high-energy electrons

P. L. Grande, M. Vos, D. K. Venkatachalam, S. K. Nandi, and R. G. Elliman

Citation: Applied Physics Letters **103**, 071911 (2013); doi: 10.1063/1.4818637
View online: http://dx.doi.org/10.1063/1.4818637
View Table of Contents: http://scitation.aip.org/content/aip/journal/apl/103/7?ver=pdfcov
Published by the AIP Publishing

Determination of thickness and composition of high-k dielectrics using high-energy electrons

P. L. Grande,[1,2] M. Vos,[3] D. K. Venkatachalam,[1] S. K. Nandi,[1,4,5] and R. G. Elliman[1]
[1]*Department of Electronic Materials Engineering, Research School of Physics and Engineering, The Australian National University, Canberra ACT 0200, Australia*
[2]*Instituto de Física, Universidade Federal do Rio Grande do Sul, Porto Alegre, RS, Brazil*
[3]*Atomic and Molecular Physics Laboratory, Research School of Physics and Engineering, The Australian National University, Canberra ACT 0200, Australia*
[4]*Research School of Astronomy and Astrophysics, The Australian National University, Canberra ACT 2611, Australia*
[5]*Department of Physics, University of Chittagong, Chittagong 4331, Bangladesh*

(Received 28 June 2013; accepted 29 July 2013; published online 15 August 2013)

We demonstrate the application of high-energy elastic electron backscattering to the analysis of thin (2–20 nm) HfO_2 overlayers on oxidized Si substrates. The film composition and thickness are determined directly from elastic scattering peaks characteristic of each element. The stoichiometry of the films is determined with an accuracy of 5%–10%. The experimental results are corroborated by medium energy ions scattering and Rutherford backscattering spectrometry measurements, and clearly demonstrate the applicability of the technique for thin-film analysis. Significantly, the presented technique opens new possibilities for nm depth profiling with high spatial resolution in scanning electron microscopes. © *2013 AIP Publishing LLC*. [http://dx.doi.org/10.1063/1.4818637]

Determining the composition of thin films as a function of depth is essential for many technological applications. HfO_2 is a technologically important metal oxide due to its use as high-k gate oxide in Metal Oxide Semiconductor (MOS) technology[1] and also in emerging resistive switching devices.[2] Many experimental techniques have been developed to characterize such layers using incident photons, electrons, or ions, each having their specific advantages and limitations. X-ray photoemission spectroscopy (XPS) is most widely used for extremely thin layers (up to few nm) and Medium Energy Ions Scattering (MEIS) and Rutherford Backscattering Spectrometry (RBS) for thicker layers.[3] Nowadays, photoemission based on hard x-rays has been developed to probe deeper below the surface, but such experiments can only be done at a few specialized synchrotron beam lines. Here, we demonstrate an alternative route, based on high-energy electron scattering, for depth profiling of very thin to relatively thick layers and for obtaining information on the electronic structure of the layer.

In XPS, the spectra are determined by the photoemission cross-section, core-level binding energies and the inelastic electron mean free path (IMFP). In ion scattering techniques, the elements are resolved due to the mass-dependence of the energy transferred in a collision, and the area and shape of the spectra are determined by the elastic scattering cross section and stopping power (energy loss per unit trajectory length), respectively. Here, we demonstrate that electron scattering at high energies (here 40 keV) can be used for depth profiling of thin HfO_2 films deposited on SiO_2 substrates. This technique is based on the IMFP (as for XPS) and elastic scattering cross sections (as for RBS) and we refer to it as ERBS (electron RBS).[4] In ERBS, separation of the elements is accomplished as in RBS by calculating the energy transfer from the electron to a nucleus assuming a collision between free particles. The fact that this is possible is somewhat surprising as the transferred energy (recoil energy) is of the order of the atomic binding energy but this approach is corroborated by experimental outcomes. Here, ERBS resembles neutron Compton scattering[5] where neutrons with kinetic energy of the order of 10 eV transfer similar amounts of recoil energy to target atoms. Since the incident particle loses energy according to well-known two-body kinematics,[4] it can be used to identify the mass of the scattering atom as long as the contributions of different elements can be resolved. Therefore, high-energy electrons as well as high-energy resolution ($\Delta E/E$ of the order of 10^{-5}) are required. As in RBS, the intensity of the elastic peaks is proportional to the elastic scattering cross-section of each atomic species and their concentration. In contrast to RBS, only the trajectories without any inelastic events (i.e., electronic excitations) are used for the compositional analysis. This is because the typical electronic excitation energy is larger than the recoil energy, whereas in RBS and MEIS, this is not the case. Longer electron trajectories contribute less to the elastic peak as the likelihood of electronic excitations occurring increases with path length. Therefore, the intensity of an elastic peak depends also on the IMFP, making depth profiling possible in a similar way as in XPS. Thus, the main features of the ERBS are the use of elastic cross-sections and kinematic factors as in the ion scattering and the electron IMFP as in photoemission. The technique is more suitable when the elastic peaks are well separated and free from a significant background due to inelastic excitations.

As is the case for neutron Compton scattering,[5] the width of the ERBS elastic peaks is not just determined by the experimental resolution but also by Doppler broadening due to the momentum distribution (thermal vibration) of the scattering atom. The Doppler broadening is given by $\sigma = (4/3\, E_{rec}\, E_{kin})^{1/2}$ with E_{kin} being the mean kinetic energy of the scattering atom and E_{rec} being the position of the elastic peak (see Table I for typical values for E_{rec} and E_{kin}). Doppler broadening has been identified as a contributing factor in the ultimate

TABLE I. Parameters used to simulate the ERBS spectrum from Eqs. (1)–(3) for 40 keV electrons. Peak position was taken from the relativistic kinematical factor.[4] The peak width (FWHM) is taken from the mean kinetic energy according to Ref. 4. IMFP values of 33 m and 55 nm for HfO_2 and SiO_2, respectively, were used.

Element	Cross-section σ_x (cm^2 /sr)	Relative to Rutherford	Concentration C_x (10^{22} atoms/cm^3)	Peak position (eV)	Peak FWHM (eV)	Mean kinetic energy (meV)
Hf	1.23×10^{-20}	1.92	2.77	0.44	0.4	38
Si	2.18×10^{-22}	0.92	2.33	2.78	1.2–1.3	68–78
O	6.87×10^{-23}	0.89	5.53 (HfO_2) 4.66 (SiO_2)	4.88	1.5–1.6	60–68

energy resolution of nuclear-reaction profiling[6] and MEIS,[7] but often totally dominates the peak width observed in ERBS. In this case, improvements in energy resolution will not reduce the measured peak widths. The peak separation increases linearly with electron energy E_0 but the peak width only with the square root of energy, hence peak resolution improves only slowly with E_0. Nevertheless, for most metal oxides on Si, the elemental peaks are well separated and in the case of large band gap oxides (such as HfO_2 and SiO_2) the peaks are free of background since the energy loss range of interest is less than the band gap. Details of the ERBS technique may be found elsewhere[4] and the experimental setup is thoroughly described in Ref. 8. In short, an electron beam with a small thermal spread is obtained using an electron gun with a BaO cathode. Slit lenses are used to focus and decelerate the electron beam from the scattering energy to the pass energy of (nominal) 200 eV. A 0.2 mm wide conical slit aperture, placed 130 mm away from the sample, determines which electron enter the analyzer. This means that the scattering angle is well determined (within 0.1°) and thus it is possible to explore geometries where the outgoing trajectory is extremely glancing with the surface. The energy resolution of the system is close to 0.3 eV full-width half maximum (FWHM). In case of insulator samples, charging may change effectively the value of the incoming energy but its influence is marginal. For example, charging by 200 eV will affect the elastic peaks separation by only 0.5% at 40 keV.

HfO_2 films were fabricated on thermally oxidized (300 nm SiO_2) silicon wafers (100 mm p-type, (100) oriented) using an atomic-layer deposition (ALD) system. Films of 2–40 nm thickness range were deposited using a Cambridge NanoTech Savannah ALD system. Substrates were held at 200 °C during deposition, and the HfO_2 layer was grown using alternating pulses of pure tetrakis-(dimethylamido)-hafnium ($Hf(NMe_2)_4$) and H_2O vapor, with an N_2 purge of the reaction chamber between pulses. After deposition, the wafers were diced into 1×1 cm square samples. These were then loaded in the spectrometer without further processing. In addition to ERBS measurements, the samples were characterized "in house" by RBS and Atomic Force Microscopy (AFM) and by MEIS at the Institute of Physics of the Federal University of Rio Grande do Sul (Brazil).

In Fig. 1, we show ERBS spectra for thick films of HfO_2 and SiO_2 for $E_0 = 40$ keV taken at normal incidence and a scattering angle of 135.5°. The corresponding recoil energies for scattering from free Hf, Si, and O atoms are reproduced in Table I. Indeed, as seen in Fig. 1, each ERBS spectrum consists of two peaks with a peak separation as predicted by Table I. The huge elastic cross-section difference between Hf and O is reflected in their peak height. The SiO_2 and HfO_2 spectra were normalized such that the area of the oxygen peaks is the same. Also evident in the spectrum from HfO_2 is an increase in scattering for energy losses greater than 6.1 eV. This is due to electrons that scatter elastically from Hf and also create an electronic excitation. The minimum energy loss for electron excitation in HfO_2 is set by the band gap for which values are reported around 5.7 eV.[9] The 6.1 eV onset thus corresponds to an energy loss of 0.4 eV due to elastic scattering from Hf and an additional 5.7 eV due to band-to-band electronic transitions in HfO_2. The inset of Fig. 1 shows similar data for $E_0 = 5$ keV. Now the elastic peaks are not resolved and the onset of electronic excitations at the band gap energy of HfO_2 and SiO_2 is seen more clearly. The ability to measure inelastic processes, such as plasmon resonances and band gaps, in addition to the ERBS peaks is very attractive. In this case, the energy spectrum resembles the one from Electron Energy Loss Spectroscopy (EELS) shifted by recoil energies.[10] From the ratio of the elastic peak areas, we confirm the stoichiometry 1:2 within 5% for both oxides using NIST electron elastic-scattering

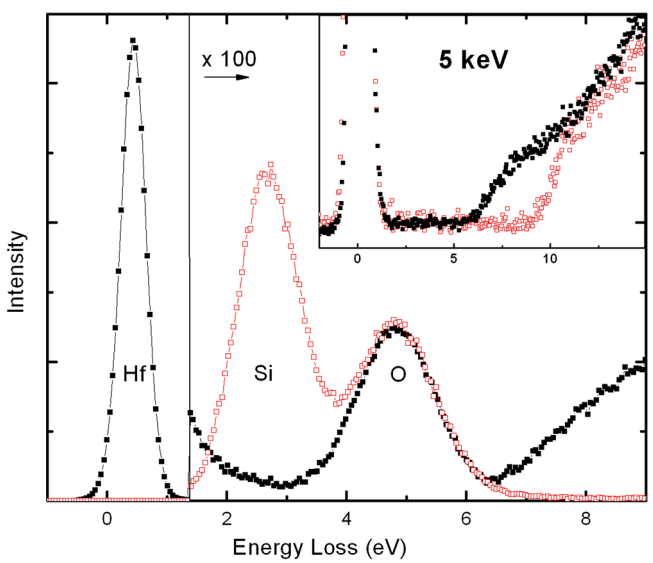

FIG. 1. Measurements of 40 keV electrons with normal incidence backscattered at 135.5° from Hafnia (closed squares) and Silica (open squares) bulk samples. For Hafnia, the intensity of the Hf elastic peak was divided by 100 for a better visualization. The inset shows the same but for 5 keV electrons.

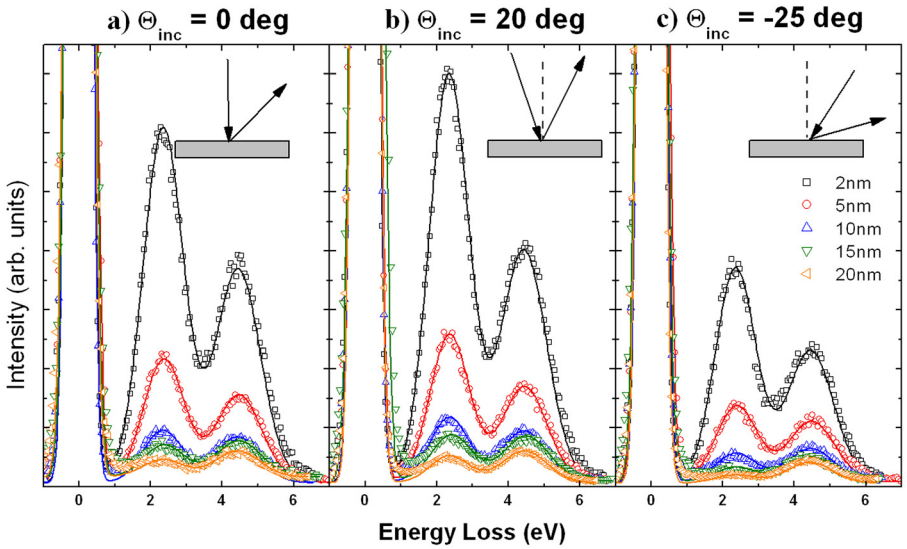

FIG. 2. Energy loss spectra taken with 40 keV electrons on different HfO_2 overlayers on SiO_2 for normal (a), tilted (b), and (c) incidences according to sketches displayed in the figure. The Hf peaks were normalized to the same area and the solid lines correspond to the best fit of the data according to Eqs. (1)–(3).

cross-section database,[11] which is based on the relativistic Dirac partial wave analysis by Salvat and coworkers as described in Ref. 12 (see Table I). It is worthwhile to point out that the stoichiometry analysis does not depend on the IMFP since this cancels out when taking the ratio of intensities for homogeneous materials. However, for the analysis of HfO_2 films on SiO_2, knowledge of the IMFP in *both* media turns out to be important, as discussed later.

Fig. 2 shows electron energy loss spectra taken at 40 keV for HfO_2 films of different thicknesses on SiO_2, and different geometries while keeping the scattering angle at 135.5°. The Hf elastic peaks were normalized to the same area. In addition to spectra taken at perpendicular incidence, (Fig. 2(a)), we also show spectra for two other geometries, chosen to maximize bulk-sensitivity (Fig. 2(b)) and surface-sensitivity (Fig. 2(c)). Each ERBS spectrum in Fig. 2 can be described as a linear combination of the spectra of HfO_2 and SiO_2 depicted in Fig. 1. Assuming an exponential attenuation for the elastic peak due to inelastic excitation along the incoming and outgoing paths, the intensities I_{Hf}, I_{Si}, and I_O for a HfO_2 layer on SiO_2 are given by

$$I_{Hf} = \alpha\, C_{Hf}\sigma_{Hf}\lambda_{HfO2}\, t/t_{eff}(1-\exp(-t_{eff}/\lambda_{HfO2})), \quad (1)$$

$$I_{Si} = \alpha\, C_{Si}\sigma_{Si}\lambda_{SiO2}\, t/t_{eff}\exp(-t_{eff}/\lambda_{HfO2}), \quad (2)$$

$$I_O = \alpha\,\sigma_O\, t/t_{eff}(C_O^{HfO2}\lambda_{HfO2}(1-\exp(-t_{eff}/\lambda_{HfO2}) + C_O^{SiO2}\lambda_{SiO2}\exp(-t_{eff}/\lambda_{HfO2})), \quad (3)$$

respectively, where σ_x and C_x are the elastic cross-section and concentration for the element x. Note that there are two concentrations (C_O^{HfO2}, C_O^{SiO2}) for O atoms. The IMFPs in SiO_2 and HfO_2 are denoted by λ_{HfO2} and λ_{SiO2}, respectively, and $t_{eff} = t(1/\cos(\Theta_1) + 1/\cos(\Theta_2))$ is the maximum trajectory length through an overlayer of thickness t. Θ_1 and Θ_2 are the angles of incidence and detection relative to the surface normal, and α is a common constant that depends on time, current, spectrometer solid angle and detector efficiency.

The solid curves shown in Fig. 2 are the best fit to the experimental data. They correspond to a sum of Gaussian functions for each element with area given by Eqs. (1)–(3) and displaced by the kinematical energy loss (see values in Table I). All parameters used for the fitting are displayed in Table I. The peak widths for Hf and O in HfO_2 and Si and O in SiO_2 were determined separately from a spectrum of thick SiO_2 with 40 nm HfO_2 and without HfO_2 layers. In fitting the measured spectra, the only free parameters were the thickness of the HfO_2 layer and the overall normalization constant α. The resulting thicknesses for the HfO_2 layers are shown in Table II together with results obtained by other techniques. Within the accuracy of the measurement, it was possible to fit the 3 spectra of Figs. 2(a)–2(c) with the same film thickness. This is consistent with the assumption of a layer-by-layer growth mode during atomic layer deposition. For other growth modes, such as islanding, the Si signal would be attenuated much less than predicted by Eq. (2) especially for the samples with thicker HfO_2 layers. The roughness of the films as measured by AFM is shown in Table II, and is typically about 5% of the film thickness.

We used the stoichiometry 1:2 for fitting spectra from both oxides and estimate an error of about 5%–10%. Table II also shows good agreement between the nominal and measured film thicknesses, with deviations of the order of 5% related to either the film preparation or to uncertainties from the ERBS analysis related to the use of Gaussian peak shapes and background effects associated with spectrometer aberrations and/or inelastic excitations. Some systematic errors may also arise from the values used for IMFPs. Here we used IMFPs calculated from the Tanuma, Powell, Penn formula (TPP2M),[13] but for the present energy this approach is an extrapolation (theory-guided) of experimental data measured at much lower energies. A careful analysis of

TABLE II. Results for the thicknesses of HfO_2 films on SiO_2 according to ERBS, RBS, and MEIS techniques.

Nominal (nm)	ERBS (nm)	RBS (nm)	MEIS (nm)	AFM σ (nm)
2	2.1	1.8	1.9	0.18
5	5.6	4.7	—	0.16
10	10.2	9.0	10.5	0.27
15	14.6	13.7	—	0.31
20	19.0	19.2	20.5	0.30

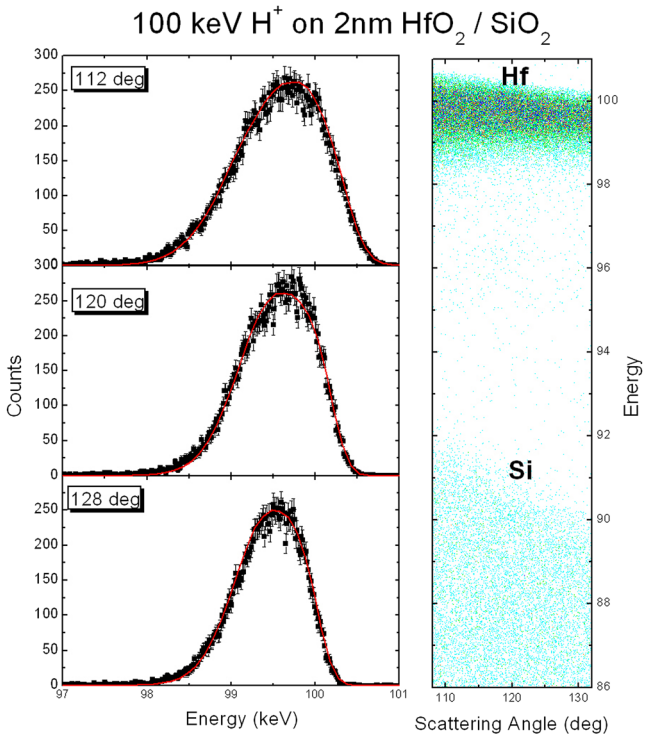

FIG. 3. Typical MEIS spectra for 100 keV H^+ on the 2 nm HfO_2 sample. The incoming beam is along the surface normal. On the right, the 2D map of scattering intensities as a function of detected energy at scattering angle. On the left, the corresponding intensities are plotted as a function of energy for three scattering angles.

Eqs. (1)–(3) shows that for very thin films the results depend mainly on λ_{SiO2}, while for thicker HfO_2 films they depend on both λ_{HfO2} and λ_{SiO2}. We estimate the uncertainty in λ_{SiO2} and λ_{HfO2} to be of the order of 10% at the high electron energies used here.

For comparison, selected samples were also analyzed by standard RBS and MEIS. For RBS, the energy loss in the thin HfO_2 layer is not resolved and the thickness of the layer is determined from the Hf peak area relative to height of the Si contribution in SiO_2. In MEIS, the energy loss in the HfO_2 layer is resolved and the film thickness can be obtained directly from the width of the Hf peak.

Fig. 3 shows the MEIS results for 100 keV H^+ on the 2 nm HfO_2 sample for three different scattering angles. A straightforward analysis based on simulations using the PowerMeis software[14] is shown as a line in Fig. 3, which shows good agreement with the measured data assuming a homogeneous film of uniform thickness and with an abrupt SiO_2/HfO_2 interface. The same holds true for the other measured samples. The MEIS and RBS results are also summarized in Table II. For both analyses, we use the stopping power from SRIM[15] and in the MEIS case straggling values close to the Yang-O'Connor-Wang formula.[16] The results confirm the ERBS analysis which highlights that the input parameters used for the ERBS analysis, namely, the IMFPs from TPP2M formula[13] and elastic cross-sections from NIST database[11] are accurate enough to allow reliable depth profiling. It should be noted that pure Rutherford cross-sections could not be used for depth profiling of heavy elements. As shown in Table I, the estimate of the scattering cross section from the Rutherford formula is approximately correct for O and Si but deviates significantly for Hf (by a factor of about two). The use of Rutherford cross sections would therefore lead to major differences between the thickness (and stoichiometry) determined by ERBS and the RBS and MEIS results.

In summary, we have demonstrated the application of the ERBS technique to the characterization of thin HfO_2 layers, showing that the techniques is capable of quantitative composition and thickness determination for films of thickness up to 20 nm, a thickness that is determined by the IMFP at the incoming energy. The technique is based on relatively simple equipment and has the potential to be integrated in a scanning electron microscope (SEM) where the use of a focused electron beam would enable laterally resolved analysis.

One of the authors (P.L.G) acknowledges the Brazilian agency CAPES (proc. 102209/12-3) for the financial support. We also thank L. F. Rosa for the assistance in the MEIS measurements in Brazil. This work is made possible by a grant of the Australian Research Council. The author (S.K.N.) gratefully acknowledges RSAA for the scholarships received for his Ph.D. studies.

[1]L. Pereira, P. Barquinha, E. Fortunato, R. Martins, D. Kang, C. J. Kim, H. Lim, I. Song, and Y. Park, Thin Solid Films **516**(7), 1544 (2008); X. Wu, D. B. Migas, X. Li, M. Bosman, N. Raghavan, V. E. Borisenko, and K. L. Pey, Appl. Phys. Lett. **96**(17), 172901 (2010).
[2]R. Waser and M. Aono, Nature Mater. **6**(11), 833 (2007); S. Lee, W.-G. Kim, S.-W. Rhee, and K. Yong, J. Electrochem. Soc. **155**(2), H92 (2008).
[3]D. P. Woodruff and T. A. Delchar, *Modern Techniques of Surface Science* (Cambridge University Press, Cambridge, 1994).
[4]M. R. Went and M. Vos, Nucl. Instrum. Methods Phys. Res. B **266**(6), 998 (2008).
[5]G. I. Watson, J. Phys. Condens. Matter **8**(33), 5955 (1996).
[6]B. Maurel, G. Amsel, and J. P. Nadai, Nucl. Instrum. Methods Phys. Res. **197**(1), 1 (1982).
[7]W. H. Schulte, B. W. Busch, E. Garfunkel, T. Gustafsson, G. Schiwietz, and P. L. Grande, Nucl. Instrum. Methods Phys. Res. B **183**(1-2), 16 (2001).
[8]M. R. Went, M. Vos, and R. G. Elliman, J. Electron Spectrosc. Relat. Phenom. **156–158**, 387 (2007).
[9]M. C. Cheynet, S. Pokrant, F. D. Tichelaar, and J. L. Rouviere, J. Appl. Phys. **101**(5), 054101 (2007).
[10]M. Vos and M. R. Went, J. Electron Spectrosc. Relat. Phenom. **162**(1), 1 (2008).
[11]C. J. Powell, A. Jablonski, and F. Salvat, Surf. Interface Anal. **37**(11), 1068 (2005).
[12]F. Salvat, A. Jablonski, and C. J. Powell, Comput. Phys. Commun. **165**(2), 157 (2005).
[13]S. Tanuma, C. J. Powell, and D. R. Penn, Surf. Interface Anal. **21**(3), 165 (1994).
[14]M. A. Sortica, P. L. Grande, G. Machado, and L. Miotti, J. Appl. Phys. **106**(11), 114320 (2009).
[15]J. F. Ziegler, M. D. Ziegler, and J. P. Biersack, Nucl. Instrum. Methods Phys. Res. B **268**(11–12), 1818 (2010).
[16]Q. Yang, D. J. Oconnor, and Z. G. Wang, Nucl. Instrum. Methods Phys. Res. B **61**(2), 149 (1991).